Numerical Simulations of Static Tested Ramjet Dump Combustor

Afroz Javed & Debasis Chakraborty

Journal of The Institution of Engineers (India): Series C
Mechanical, Production, Aerospace and Marine Engineering

ISSN 2250-0545

J. Inst. Eng. India Ser. C
DOI 10.1007/s40032-016-0312-3

Springer

J. Inst. Eng. India Ser. C
DOI 10.1007/s40032-016-0312-3

ORIGINAL CONTRIBUTION

Numerical Simulations of Static Tested Ramjet Dump Combustor

Afroz Javed[1] · **Debasis Chakraborty**[1]

Received: 1 September 2015 / Accepted: 23 May 2016

Abstract The flow field of a Liquid Fuel Ram Jet engine side dump combustor with kerosene fuel is numerically simulated using commercial CFD code CFX-11. Reynolds Averaged 3-D Navier–Stokes equations are solved alongwith SST turbulence model. Single step infinitely fast reaction is assumed for kerosene combustion. The combustion efficiency is evaluated in terms of the unburnt kerosene vapour leaving the combustor. The comparison of measured pressures with computed values show that the computation underpredicts (∼5 %) pressures for non reacting cases but overpredicts (9–7 %) for reacting cases.

Keywords Ramjet dump combustor · Liquid fuel ramjet · CFD

Introduction

In ducted rockets and volume limited ramjet engine based missiles, booster rocket is integrated into ramjet combustor to minimize missile volume and dump combustor is employed for ramjet phase of operation. The dump combustors do not have conventional flame holders, and the flame stabilization depends upon the recirculation zones formed by the sudden enlargement of the flow area between the inlet duct and combustion chamber. Figure 1 shows such a dump combustor where the side mounted air inlets supply air for combustion. The flow fields occurring in such side dump combustors are complex and three-dimensional. The flow field in the immediate vicinity of the jets from inlet ducts consists of complex three-dimensional vortex regions. The flow is characterized by a recirculating zone between the dome and the inlets, which arises by the combination of spill-over flow and shear with the inlet jets. In far downstream regions of the inlets, the flow becomes mainly axial and the counter rotating vortices in the cross-section decay progressively with axial distance. The flow patterns have significant influence on the fuel dispersion, combustion characteristics and local heating rates in the combustor.

A few experimental studies [1–3] are reported in literature to understand the reacting and non reacting flow fields of side dump combustors. These experimental studies show flow features which are specific to the model geometry considered and no general scaling law exists to extend the observations from these experiments to the combustors with altered geometries. Numerical studies are conducted by many researchers [4–7] to understand the complex flow field by considering only single component fluid. A numerical study of mixing of ethylene fuel in a side dump combustor is carried out by some of the prior investigators [8]. The effect of side inlet angles on the mixing is analysed as given [9] in another study. The researchers have [10] numerically analysed the mixing and combustion characteristics of fuel rich solid propellant in a side dump combustor. The numerical study of mixing and combustion of liquid fuel in a side dump combustor is not reported in the open literature to the best of the knowledge of the authors. In the present work, reacting and non-reacting flow fields of a liquid fuelled side dump ramjet combustor are analysed numerically. In this combustor, air is supplied through two intake ducts as shown in Fig. 1. The exit nozzle of the engine has only convergent portion for the purpose of static test. Once the air flow is established, a hydrogen combustor in the air supply path is

✉ Afroz Javed
afrozjaved@gmail.com

[1] Computational Combustion Dynamics/Directorate of Computational Dynamics, Defence Research and Development Laboratory, Hyderabad 500058, India

Published online: 29 June 2016

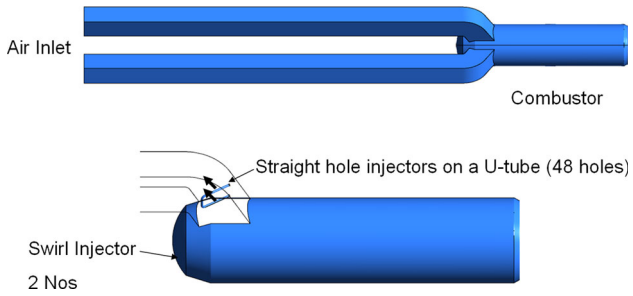

Fig. 1 Geometry with locations of injectors for LFRJ static test engine

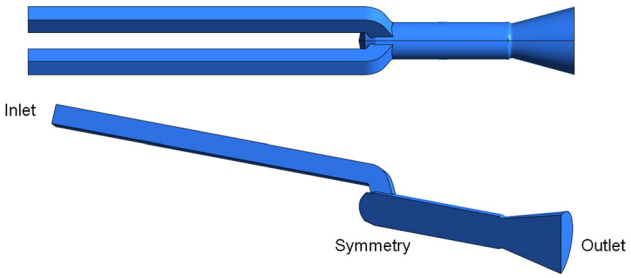

Fig. 2 Computational geometry and boundaries

turned on to heat the air. The combustion of hydrogen causes vitiation of the air with increase in water vapour percentage and a slight decrease in oxygen percentage (21.45 % from original 23 % by mass). Kerosene fuel is injected in hot air through straight hole fuel injectors in the intake duct and two swirl injectors at the combustor dome. An igniter with a solid charge at the combustor dome initiates ignition. During the test, static pressures are monitored at different locations.

Computational Fluid Dynamics (CFD) simulations are carried out to evaluate the chamber pressure and combustion efficiency in terms of unburnt fuel. Due to the change in the inlet air flow, fuel flow and igniter flow, five different flow situations are identified, namely,

- Only atmospheric air flow through intake ducts
- Vitiated air flow
- Fuel flow turned on in the vitiated air flow
- Igniter turned on
- Igniter turned off

Quasi steady state simulations for different flow conditions are carried out in the present work and the results are analysed.

Computational Geometry, Boundaries, and Flow Parameters

Since the static tested engine contains only convergent portion of the nozzle, it is required to include a large domain size in the atmosphere to give a correct boundary condition. In order to avoid inclusion of such large domain in atmosphere, a divergent extension is provided for the purpose of numerical simulations as shown in Fig. 2. Since the flow becomes supersonic in the divergent portion, the low pressure or supersonic boundary conditions applied at the exit of the divergent portion do not affect the combustor flow field. Only half of the geometry is considered from the consideration of symmetry. The locations of different boundaries are also shown in Fig. 2.

Table 1 Flow parameters for simulations

Parameter	Value
Air flow rate	11.2 kg/s
Air intake static pressure	4.5 bar
Fuel flow rate in dump region	0.48 kg/s
Fuel flow rate in dome region	0.08 kg/s
Temperature of air	540 K
O_2 mass fraction	0.21455
H_2O mass fraction	0.01853
CO_2 mass fraction	0.00048

The flow parameters are shown in Table 1 for the simulations. It can be observed that the vitiated air has got slightly lower oxygen content than the atmospheric air with a small amount of water vapour (1.85 %). The fuel used is Jet-A with equivalent chemical formula $C_{12}H_{23}$.

Governing Equations and Models

The flow in a liquid fuel ramjet combustor can be described as chemically reacting, multi phase, and multi species flow. Mass continuity equation, Navier–Stokes Equations, energy equation, and (n − 1) species mass fraction equations (n is the number of species considered) are the governing equations for single phase flows. A multiphase flow containing dispersed particles may be modeled using either the particle transport (Lagrangian Particle Tracking) model or the Eulerian–Eulerian multiphase model.

A commercial software CFX-11 [11] is used to solve the governing equations. To find out the accuracy and the range of applications, the software has been validated for various internal flow fields in the rectangular duct behind backward facing step [12, 13], base flow [14], free jets [15], free stream and jet interaction [16–18], dual pulse rocket motor [19], air intakes [20] etc. and good quantitative agreement has been obtained between experimental and computational results. The software has also been validated for the reacting flow fields with Hydrogen

[21–24] combustion in air as well as liquid kerosene [25–29] combustion, and good quantitative matches with the experimental values are reported.

The code is fully implicit, using finite volume method with finite element based discretization of geometry. In the present study the convective terms are discretized through 2nd order scheme. Turbulence is modelled by using Shear Stress Transport (SST) turbulence model proposed by the researchers [30]. The SST turbulence model is derived by blending $k-\omega$ and $k-\varepsilon$ turbulence models through a blending function. In this blended turbulence model the robust and accurate formulation of $(k-\omega)$ model in the near wall region is retained, while taking advantage of the free stream independence of the $(k-\varepsilon)$ model in the outer part of the boundary layer. The details of the governing equations for single phase flow field with SST turbulence model are described in detail by earlier investigators [22]. This turbulence model has shown very good wall pressure and drop in total pressure predictions for both non reacting [19, 31], and reacting [22] flow simulations dealing with internal flow situations carried out by the authors.

The Reynolds/Favre averaging of energy and species equations give rise to additional unclosed terms as Reynolds heat and species mass flux vectors. These unclosed terms are modeled through the concept of turbulent Prandtl and turbulent Schmidt numbers. A few researchers [32–35] have suggested use of complicated additional transport equations for the modeling of turbulent Prandtl/Schmidt numbers in the propulsive flows. The researchers [36] have carried out model free simulations for compressible and incompressible mixing layers and shown that the turbulent Prandtl/Schmidt numbers do not vary significantly for incompressible cases while observing a continuous variation of these numbers in compressible cases. Many numerical studies [37–39] carried out for subsonic combustor performance, have also shown that assumption of constant turbulent Prandtl/Schmidt numbers can give good prediction of the flow variables. In the present case also constant values of turbulent Prandtl/Schmidt numbers are considered and set as equal to 0.9.

Multi Phase Model

The kerosene fuel is injected from straight hole as well as swirl injectors in liquid form. The fuel jet rapidly disintegrates in small liquid droplets, which travels in the gaseous flow with vapourisation. The motion of the liquid droplets can be modelled through either Eulerian–Eulerian methodology for both the phases or Lagrangian methodology to track the motion of droplets. In the present case Lagrangian tracking for the particle motion is used, as it is best suited for low particle volume fraction in the flow. The particle volume fraction with a density of 800 kg/m^3 for Jet-A fuel comes out to be nearly 0.018 %, for the present case, which is very small and Lagrangian particle tracking can be used effectively.

Lagrangian tracking involves the integration of droplet paths through the discretized domain. Individual droplets are tracked from their injection point until they escape the domain or vaporise completely according to the vaporisation model used. The forces acting on the particle which affect the particle acceleration are due to the difference in velocity between the particle and fluid, displacement of the fluid by the particle, gravitational force, buoyancy, and forces arising due to rotation of the frame of reference. For the case under consideration, due to very small particle size, relatively small residence period, and non rotating frame of reference, only aerodynamic forces are dominant. The aerodynamic force acting on the particle is given as follows,

$$F_D = \frac{1}{2}\rho_g\left(V_g - V_p\right)\left|\left(V_g - V_p\right)\right|C_D S$$

where, ρ_g is gaseous medium density, V_g is gas velocity, V_p is the velocity of particle, S is the frontal area of the particle, and C_D is drag Coefficient which may be evaluated by using Schiller and Naumann [40] drag coefficient equation given as following,

$$C_D = \frac{24}{Re}\left(1.0 + 0.15Re^{0.687}\right)$$

This equation is modified by ANSYS CFX [11] to ensure the limiting behavior in the inertial regime as given below,

$$C_D = \max\left[\left\{\frac{24}{Re}\left(1.0 + 0.15Re^{0.687}\right)\right\},\ 0.44\right]$$

After the evaluation of trajectory of individual particle, an average of all particle tracks is obtained to generate source terms to the fluid mass, momentum, and energy equations.

Vaporisation Model

During its travel the liquid droplet undergoes vaporization. The liquid evaporation model is a model for particles with heat transfer and one component of mass transfer (that is from liquid to gas only), and in which the continuous gas phase is at a higher temperature than the particles. The model uses two mass transfer correlations depending on whether the droplet is above or below the boiling point. This is determined through the Antoine equation given as,

$$\ln\left(\frac{p_{vapour}}{p_{ref}}\right) = A - \frac{B}{T + C}$$

where A is the Antoine reference state constant, B is the Antoine enthalpic coefficient and C is the Antoine

temperature coefficient. These values for Jet-A are taken as A = 23.3, B = 5600 K and C = 25 K.

When the droplet is above the boiling point, that is vapour pressure is more than surrounding pressure, the mass transfer is determined by the convective heat transfer as given below,

$$\dot{m} = -\frac{Q_C}{L}$$

where Q_C is the convective heat transfer and L is the latent heat of boiling. When the droplet is below the boiling point, the mass transfer is given by the formula,

$$\dot{m} = \pi d_p D Sh \frac{W_C}{W_G} \log\left(\frac{1-X}{1-X_G}\right)$$

here d_p is the droplet diameter, D is the dynamic mass diffusivity, W_C and W_G are the molecular weights of the vapor and the mixture in the continuous phase, while X and X_G are the molar fractions in the droplet surface and in the gas phase. The Sherwood number is evaluated as,

$$Sh = 2.0 + 0.6 Re^{1/2} Sc^{1/3}$$

where Re is Reynolds number and Sc is Schmidt number.

Droplet Diameters and Spray Cone Angles

When the fuel is atomised through the injectors, a distribution of the droplet sizes is obtained. In order to model the droplet sizes a representative diameter, namely Sauter Mean Diameter (SMD) is defined. SMD is the diameter of a droplet whose ratio of volume to surface area is same as that of the entire spray. A good approximation can be made by using this droplet size to represent the size of an equivalent monodisperse spray for the analysis of evaporation and combustion problems [41].

The Sauter mean diameter of the droplets from straight hole injectors can be expressed as [42],

$$SMD = \frac{500 d_0^{1.2} \nu_L}{U_L}$$

The half cone angle of the spray is calculated by the jet mixing theory of Abramovich [43] as,

$$\tan\theta = 0.13\left(1 + \frac{\rho_A}{\rho_L}\right)$$

The SMD expression for swirl injector is taken from previous literature [44], and is given below as,

$$SMD = 2.25 \sigma^{2.25} \mu_L^{0.25} \dot{m}_L^{0.25} \Delta P_L^{-0.5} \rho_A^{-0.25}$$

The cone angle of spray from a pressure swirl atomizer is equal to the cone angle of the atomizer exit, which is 60° in the present case.

Combustion Modelling

The stoichiometric air to fuel ratio for Jet-A (approximated as equivalent to $C_{12}H_{23}$) is 14.97 with normal air. For the vitiated air composition used in the present case as given in Table 1, the stoichiometric air to fuel ratio comes out to be 15.85. The typical air to fuel ratio used in the combustor is around 20.00, which is towards leaner side, and hence the combustion of Jet-A fuel can be assumed to occur with a single step reaction as follows.

$$C_{12}H_{23} + 17.75O_2 \rightarrow 12CO_2 + 11.5H_2O$$

The rate of reaction depends either on kinetics or on physical mixing. Physical mixing is the process of generating a homogeneous mixture of reactants at the molecular level. Kinetics dictates the rate at which molecules of fuel and oxidiser collide with sufficient energy to react. Both of these processes are necessary for reaction to occur and rate of reaction may be controlled by either of the two processes. Owing to the comparatively lower speeds, higher temperature, and pressure the kinetic processes are expected to be very fast compared to the mixing process. Due to faster chemical processes a mixing rate controlled combustion model namely Eddy Dissipation Model (EDM) is selected to model the combustion. The reaction rate determined by the EDM is given as.

$$R_{edm} = -A\rho\frac{\varepsilon}{k}\min\left\{Y_f, \frac{Y_0}{s}, B\frac{Y_p}{1+s}\right\}$$

where Y_f, Y_0 and Y_p are the mass fractions of fuel, oxidiser, and products respectively. The mass stoichiometry of the reaction is denoted by s. A and B are model constants. The value of A is 4.0 and the value of B for single step forward reaction only, is taken as negative (−1.0), which makes the reaction rate independent of the concentration of the products species.

Computational Grids Boundary Conditions and Numerical Simulations

Hexahedral grids with clustering near flow gradients and boundary layers are generated using ICEM CFD software [45]. Different grid sizes are used to simulate the air flow only, and the centreline pressure is monitored to carry out grid independence study. Three grid sizes of 3.1, 6.4, and 8.3 million are simulated. The centreline static pressures in the combustion chamber for all the three simulations are shown in Fig. 3. The difference between 6.4 and 8.3 million grid data is found to be very small. Based on these simulations 6.4 million grid size is used for further simulations.

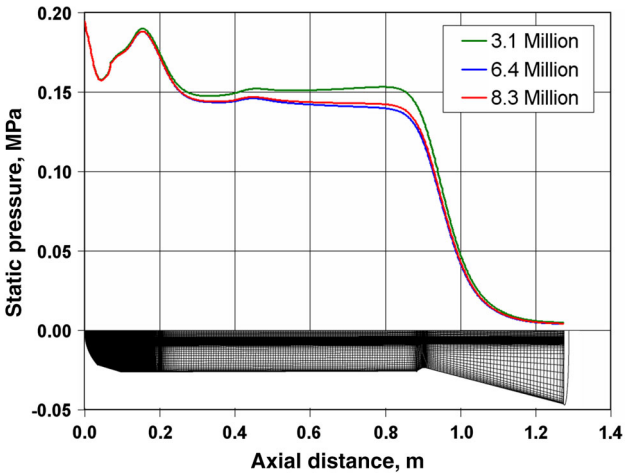

Fig. 3 Effect of grids on the centreline static pressure

Typically a mass flow rate inlet boundary is applied on the intake duct with specified total temperature and composition of the inlet air. No slip condition is applied on the walls with adiabatic condition for heat transfer. The outlet condition is given as supersonic exit. Point injection is assumed for the fuel flow from straight hole injectors (shown in Fig. 1). The centres of the holes are evaluated from the geometry and fed in the pre-processor. The direction of injection is specified by specifying the direction cosines. The Sauter mean diameter of the droplets is taken as 34 μ for straight holes injectors and 14 μ for swirl injectors. The fuel exit speed from straight hole injectors is 51 m/s and cone angle is 15°. The motion of the droplets is analysed through Lagrangian particle tracking.

The different boundary conditions for all the five quasi steady state conditions are discussed as follows.

Air On

Initially the atmospheric air is allowed to flow in the intake ducts. The temperature of the air is set as 300 K for this situation; the composition is taken same as atmospheric air condition. No fuel is injected from the injection holes.

Heater On

With the turning on of the vitiated air heater, Hydrogen is burnt with air and Oxygen is replenished in the downstream direction before the vitiated air is supplied to the intake ducts. In this stage all the inlet properties are given as shown in Table 1, except that the fuel is not injected.

Fuel On

In the hot air flow when fuel is turned on, the mass flow rate of kerosene and other required parameters like droplet diameter, spray cone angle etc. are given as fuel injection parameters with the mass flow rates as shown in Table 1. The ignition temperature of Jet-A is set at around 600 K. In the fuel on condition the fuel simply vaporizes in the hot air (540 K) flow without any chemical reaction.

Table 2 Thermo physical properties of igniter gas

Parameter	Value
Molecular weight	28.042 kg/kmol
Specific heat at constant pressure	2027.1 J/kg K
Dynamic viscosity	9.98×10^{-5} Pa.s
Thermal conductivity	0.8927 W/mK
Total temperature	3400 K

Igniter On

The mass flow rate of the igniter gases from igniter nozzle is given as one more inlet boundary in igniter on condition. The igniter gases are modelled as non reacting single species with a temperature of 3400 K with equivalent thermochemical and transport properties, as shown in Table 2. The igniter gives a constant mass flow rate of 0.12 kg/s during its operation, which is kept as an inlet boundary condition at the igniter location. Combustion of the fuel starts at the high temperatures occurring due to igniter gas.

Igniter Off

The Igniter inlet mass flow rate is set to zero and the inlet is reassigned as a wall. When the igniter is turned off, the combustion chamber is already filled with the high temperature caused by the ignition and combustion of the fuel. And sustained burning of kerosene is expected to occur.

Results and Discussions

The numerical simulations are carried out for the five different quasi steady state conditions. The particle tracks are shown in Fig. 4 for fuel on, igniter on and igniter off conditions. It is evaluated from post processing the results that when fuel is injected in hot air stream, around 89.6 % of the injected fuel vaporises by the time it reaches nozzle entry plane and rest of the 10.4 % fuel leaves in liquid state. When the igniter is turned on, due to combustion and very high temperature gases from igniter, all the fuel vaporises within a short distance inside combustor. However, all the vaporised fuel does not burn and around 1.7 % of it leaves the combustor unburnt. When the igniter is turned off, all the fuel still vaporises within a short distance

of combustor but the percentage of vapour leaving nozzle exit plane increases to around 3 %. The combustion model used assumes "mixed is burnt", for fuel vapour; the amount of the vapour leaving the combustor could be taken as a measure of inefficiency in combustion. With this consideration the combustion efficiency would be around 98.3 and 97 % for igniter on and off conditions respectively.

The axial velocity and CO_2 mass fractions at five different planes within the combustor are analysed for the development of a uniform flow field near the nozzle inlet, the axial locations of the planes considered normalized by the combustor length, are shown in Table 3.

The distribution of axial velocity at different planes, as depicted in Fig. 5, shows increased velocity for reacting flows. The maximum velocity occurring in the combustion chamber is nearly 300 m/s for non reacting flow, while it is of the order of 500 m/s for reacting cases. Examination of Fig. 5c clearly shows a more uniform flow field when the igniter is turned off.

To further analyse the development of velocity field, the uniformity is quantified in terms of average speed normalized by the maximum speed at the location of the plane. These ratios are shown in Fig. 6 for the planes considered at the different operating conditions. It is evident that the flow is very nonuniform near the dome region at plane I for all the three conditions. The very low value (0.07) for igniter on condition occurs due to near sonic speed of the igniter gases increasing the value of maximum speed at the Plane I. In the downstream direction the mixing of igniter gases occurs with the loss of high speed and more uniform velocity field is observed. Near the nozzle entry (Plane V), the velocity fields in terms of average to maximum velocity ratio are nearly similar (within 5 %) for all the three operating conditions.

The distribution of CO_2 mass fraction is shown in Fig. 7 at different axial cross sections. Like velocity distribution the CO_2 mass fraction distribution also becomes more balanced and uniform for igniter off condition.

The ratios of average CO_2 mass fraction to the maximum CO_2 mass fraction are plotted in Fig. 8 for both the igniter on and igniter off conditions at the different planes considered for the analysis. This ratio is minimum at Plane I (near the dome), and goes on increasing as the flow proceeds downstream for both the cases. The CO_2 distribution near the dome region (Plane I) is nearly equal for both the cases, a better CO_2 distribution for igniter on condition is observed up to the location of Plane III, after that the distribution of igniter off condition is better.

The static pressure distribution at the nozzle entry plane is shown in Fig. 9 for different flow conditions. It is observed that the pressure at the nozzle entry plane is quite uniform for the air on condition, when the heater is turned on the pressure increases in magnitude with negligible non uniformity. As the fuel is turned on, the pressure at the nozzle entry plane is observed to decrease slightly, while maintaining its uniformity. The flow pressure field

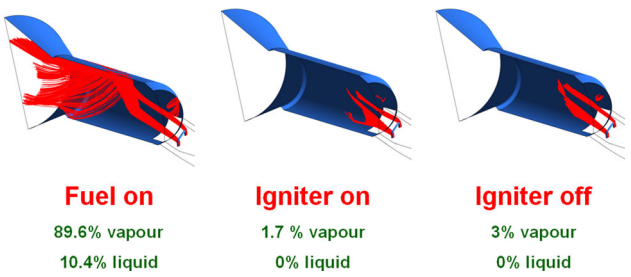

Fig. 4 Particle tracks for different conditions, percentage of kerosene vapour and liquid at the exit plane of combustor

Table 3 Axial locations of the planes

Plane No.	I	II	III	IV	V
Position from dome end (location/combustor length)	0.055	0.333	0.556	0.778	0.998

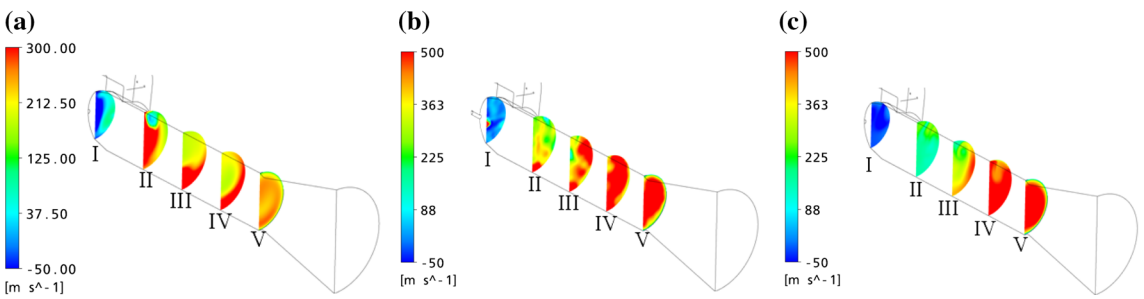

Fig. 5 Axial velocities at different cross sections for **a** fuel on **b** igniter on and **c** igniter off conditions

becomes visible nonuniform with the turning on the igniter. The pressure field returns to its uniformity after the igniter is turned off.

The static pressure at the nozzle entry plane is measured during the static test; this pressure is compared with the computed static pressure at the same location for different operating conditions in Table 4. It can be observed that the computed pressures are on slightly lower side for the non reacting cases (air on, heater on, and fuel on) while higher pressures (9–7 %) are predicted for reacting cases.

The uniformity of the pressure field at the nozzle entry plane can be expressed in terms of the ratio of average static pressure to the maximum static pressure. These ratios are shown in Fig. 10. It can be observed that this ratio remains nearly constant for, air on, heater on, and fuel on conditions, with the turning on of igniter flow, the uniformity of the flow field drops to nearly half of its initial value. This non uniformity is clearly visible in Fig. 9 also. However, when the igniter is turned off and only kerosene combustion keeps on taking place the flow uniformity

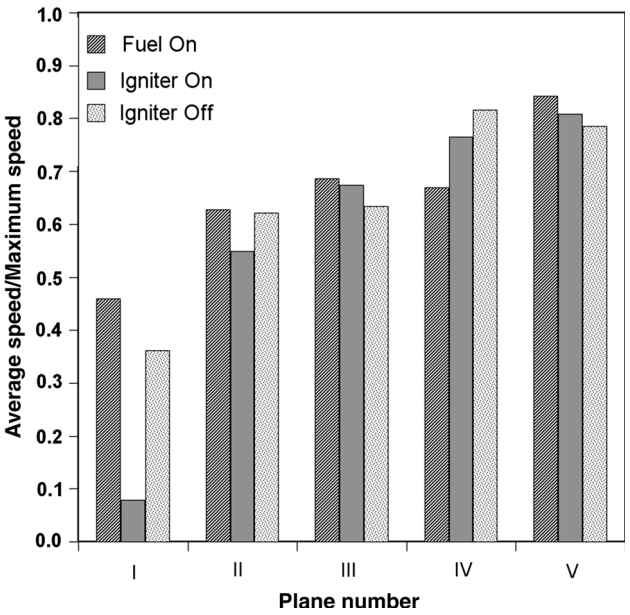

Fig. 6 Ratio of average speed to the maximum speed at the plane locations for different flow conditions

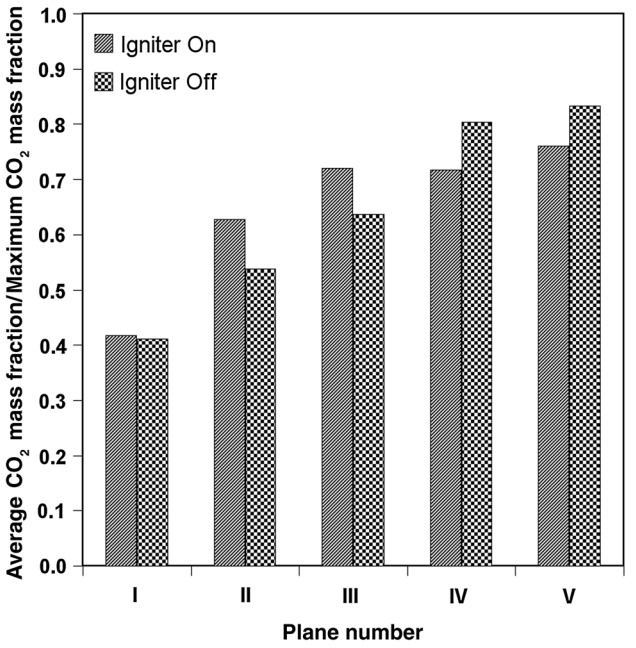

Fig. 8 Ratio of average CO_2 mass fraction to the maximum CO_2 mass fraction at the plane locations for different flow conditions

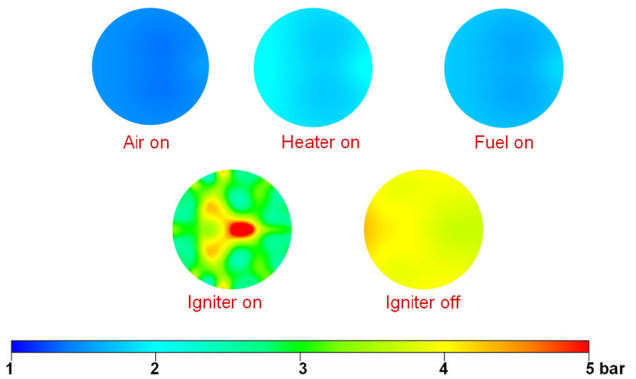

Fig. 9 Pressure distribution at nozzle entry plane

Fig. 7 CO_2 mass fractions at different cross sections for **a** igniter on and **b** igniter off conditions

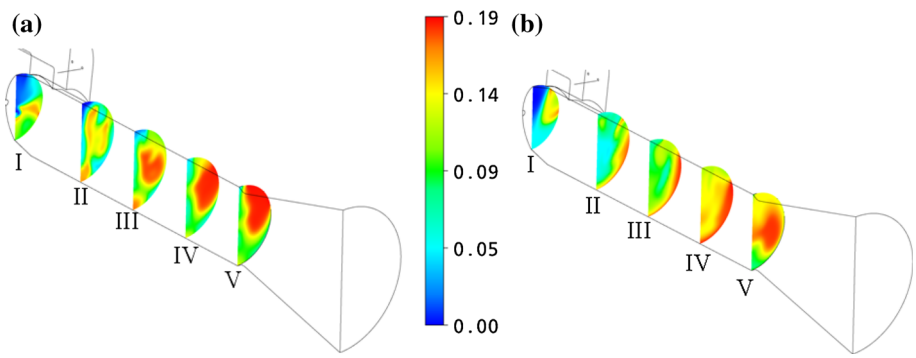

nearly returns to its original values, indicating a negligible effect on the flow uniformity due to combustion process as compared with the non reacting flow field.

The total temperature at the nozzle inlet plane is normalized by its maximum value at the same plane and the distribution is shown in Fig. 11, for igniter on and igniter off conditions. The examination of this figure clearly indicates zones of high total temperatures away from the fuel injection locations in the igniter on condition. These high temperature zones occur due to presence of high temperature igniter gases in the flow field. However, when the igniter is turned off, the high temperature zones shift to the locations of fuel injection. This information is useful from the point of view of providing insulation at these critical zones.

Table 4 Comparison of measured and computed pressures

S. No.	Flow condition	Pressure, bar		Difference, %
		Measured	Computed	
1	Air On	1.49	1.44	+3.4
2	Heater On	1.90	1.84	+3.2
3	Fuel On	1.91	1.81	+5.2
4	Igniter On	4.08	4.47	−8.7
5	Igniter Off	3.63	3.89	−6.7

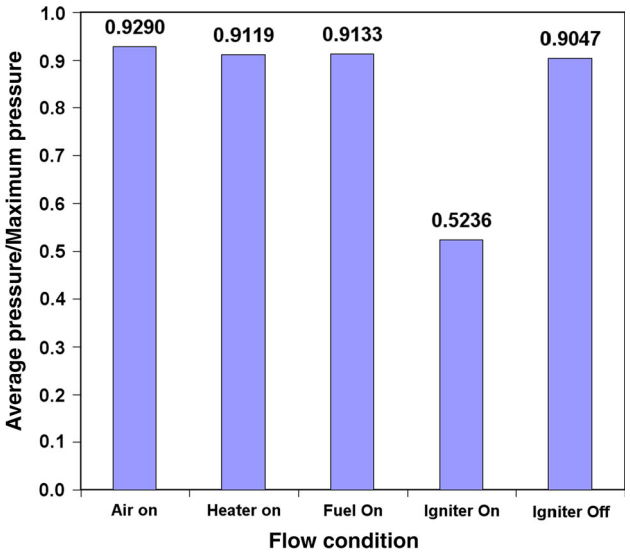

Fig. 10 Ratio of average static pressure to the maximum static pressure at nozzle entry plane for different flow conditions

Conclusion

Nonreacting and reacting simulations are carried out for a static tested Liquid Fuel Ramjet combustor using a commercial CFD code CFX-11. The complete test sequence is divided in five quasi steady state flow simulations. It is observed that around 90 % of the kerosene vaporises when injected in hot air stream. After the igniter is turned on all the kerosene vaporises within a short distance after the injection, and only 1.7 % kerosene vapour leaves the combustor, unburnt. When the igniter is turned off, the unburnt kerosene is 3 %. The flow field is seen to be uniform at the nozzle entry except for the igniter on condition. The comparison of measured pressures with that obtained from computational results shows that the computed pressures are on lower side (∼5 %) for the non reacting cases (air on, heater on, and fuel on) while higher pressures (9–7 %) are predicted for reacting cases. The analysis of velocity, CO_2 mass fraction, and pressure fields indicate a nearly uniform flow at the nozzle entry plane.

Acknowledgment This manuscript is the expanded version of the paper titled, "Numerical Simulations of Static Tested Ramjet Dump Combustor" presented in "2nd National Propulsion Conference" during February 23–24, 2015 at Indian Institute of Technology Bombay, Mumbai, India.

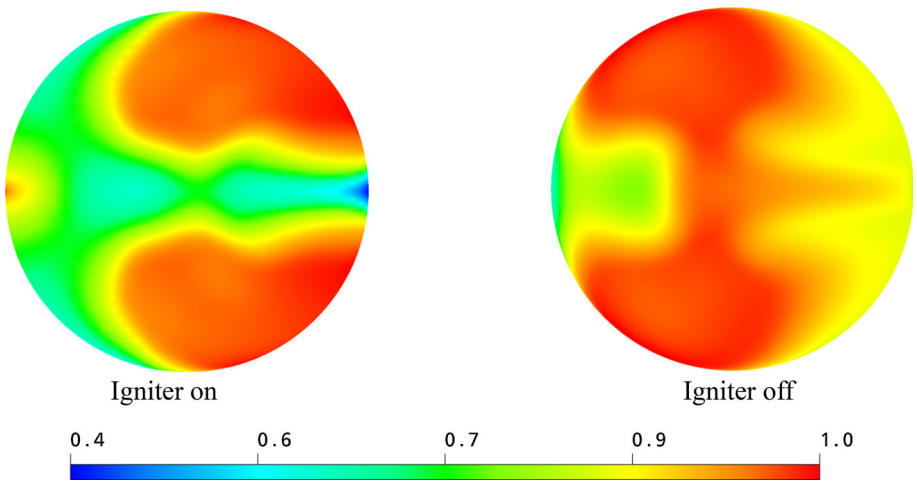

Fig. 11 Distribution of total temperature normalized by maximum total temperature at nozzle entry plane, for both igniter on and igniter off conditions

References

1. F.D. Stull, R.R. Craig, G.D. Streby, S.P. Vanka, Investigation of a dual inlet side dump combustor using liquid fuel injection. J. Propuls. Power **1**(1), 83–88 (1985)
2. T.M. Liou, S.M. Wu, Flowfield in a dual-inlet side-dump combustor. J. Propuls. Power **4**(1), 53–60 (1988)
3. T.M. Liou, H.L. Lee, C.C. Liao, Effects of guide-vane number in a three-dimensional 60-deg curved side-dump combustor inlet. J. Fluids Eng. **123**, 211–218 (2001)
4. S.P. Vanka, F.D. Stull, R.R. Craig, Analytical characteristics of flow fields in side-inlet dump combustors. AIAA Paper pp. 83–1399 (1983)
5. Z.C. Hong, T.H. Ko, A numerical study on the three-dimensional vortex motion in a side-inlet dump combustor. AIAA Paper pp. 88–3009 (1988)
6. T.M. Liou, Y.H. Hwang, Calculation of 3-D turbulent flow fields in side-inlet ramjet combustors with an algebraic Reynolds stress model. J. Propuls. Power **5**(6), 686–693 (1989)
7. R.H. Yen, T.H. Ko, Effects of side-inlet angle in a three-dimensional side-dump combustor. J. Propuls. Power **9**(5), 686–693 (1993)
8. T.H. Ko, Three-dimensional fuel–air mixing phenomena in a side-dump combustor: a numerical study. Int. Commun. Heat Mass Transf. **32**, 1360–1374 (2005)
9. T.H. Ko, A numerical study on the effects of side-inlet angle on the mixing phenomena in a three-dimensional side-dump combustor. Int Commun Heat Mass Transf **33**, 853–862 (2006)
10. D.L. Cherng, D.V. Yang, K.K. Kuo, Numerical study of turbulent reacting flows in solid-propellant ducted rocket combustors. J. Propuls. Power **5**(6), 678–685 (1989)
11. ANSYS CFX-11 Release 11, Installation and overview (2007)
12. P. Manna, D. Chakraborty, Numerical investigation of transverse sonic injection in a nonreacting supersonic combustor. Proc. Inst. Mech. Eng. G J. Aerosp. Eng. **219**(3), 205–215 (2005)
13. P. Manna, D. Chakraborty, Numerical investigation of confinement effect on supersonic turbulent flow past backward facing step with and without transverse injection. J. Aerosp. Sci. Technol. **61**(2), 283–294 (2009)
14. M. Dharavath, P.K. Sinha, D. Chakraborty, Simulation of supersonic base flow: effect of computational grid and turbulence model. ASME J. Aerosp. Eng. **224**(3), 311–319 (2010)
15. M. Dharavath, D. Chakraborty, Numerical simulation of underexpanded sonic jet. J. Aerosp. Sci. Technol. **14**(4), 259–267 (2012)
16. G. Aswin, D. Chakraborty, Numerical simulation of transverse side jet interaction with supersonic free stream. J. Aerosp. Sci. Technol. **14**(5), 295–301 (2010)
17. S. Saha, S. Rathod, M.S.R.C. Murty, P.K. Sinha, D. Chakraborty, Numerical simulation of base flow of a long range flight vehicle. Acta Astronaut. **74**(3), 112–119 (2012)
18. S. Saha, P.K. Sinha, D. Chakraborty, Numerical prediction of surface heat flux during multiple jets firing for missile control. J. Inst. Eng. (India) (Ser. C) **94**(1), 85–91 (2013)
19. A. Javed, P. Manna, D. Chakraborty, Numerical simulation of dual pulse rocket motor flow field. Def. Sci. J. **62**(6), 369–374 (2012)
20. S. Saha, P.K. Sinha, D. Chakraborty, CFD prediction of ramjet intake characteristics at angle of attack, in Proceedings of 8th National Conference on Air breathing engines and Aerospace Propulsion, 97–107 (at DIAT, Pune, India December 12–14, 2006)
21. P. Manna, D. Chakraborty, Numerical simulation of transverse H_2 combustion in supersonic air stream in a constant area duct. J. Inst. Eng. (India) **86**, 47–53 (2005)
22. A. Javed, D. Chakraborty, Numerical simulation of supersonic combustion of pylon injected hydrogen fuel in scramjet combustor. J. Inst. Eng. (India) **87**, 1–6 (2006)
23. S. Saha, D. Chakraborty, Reacting flow computation of staged supersonic combustor with strut injection. J. Aerosp. Sci. Technol. **63**(4), 289–298 (2011)
24. M. Dharavath, P. Manna, D. Chakraborty, Thermochemical exploration of hydrogen combustor in generic scramjet combustor. Aerosp. Sci. Technol. **24**, 264–274 (2013)
25. R. Behera, D. Chakraborty, Numerical simulation of kerosene fuelled ramp cavity based scramjet combustor. J. Aerosp. Sci. Technol. **58**, 104–112 (2006)
26. P. Manna, R. Behera, D. Chakraborty, Thermochemical exploration of a cavity based supersonic combustor with liquid kerosene fuel. J. Aerosp. Sci. Technol. **59**(4), 246–258 (2007)
27. P. Manna, R. Behera, D. Chakraborty, Liquid fueled strut based scramjet combustor design: a computational fluid dynamics approach. J. Propuls. Power **24**(2), 274–281 (2008)
28. D. Chakraborty, CFD based design of kerosene fueled scramjet combustor. Int. J. Hypersonics **1**(1), 14–29 (2010)
29. M. Dharavath, P. Manna, D. Chakraborty, Effect of turbulence models and spray parameters on kerosene fuelled scramjet combustor. J. Aerosp. Sci. Technol. **67**(3), 369–383 (2015)
30. F.R. Menter, Two-equation eddy-viscosity turbulence models for engineering applications. AIAA J. **32**(8), 1598–1605 (1994)
31. A. Javed, P.K. Sinha, D. Chakraborty, Numerical exploration of solid rocket motor blast tube flow field. Def. Sci. J. **63**(6), 616–621 (2013)
32. Y. Nagano, C. Kim, A two equation model for heat transport in wall turbulent shear flows. J. Heat Transf. **110**, 583–589 (1988)
33. N. Chidambaram, S.M. Dash, D.C. Kenzakowski, Scalar variance transport in the turbulence modeling of propulsive jets. AIAA **17**(1), 99–0235 (1999)
34. X. Xiao, J.R. Edwards, H.A. Hassan, A.D. Cutler, Variable turbulent Schmidt number formulation for scramjet applications. AIAA J. **44**(3), 593–599 (2006)
35. D.C. Kenzakowski, J. Papp, S.M. Dash, Evaluation of advanced turbulence models and variable Prandtl/Scmidt number methodology for propulsive flows. AIAA p. 0885 (2000)
36. A. Javed, N.K.S. Rajan, D. Chakraborty, Behaviour of turbulent Prandtl/Schmidt number in compressible mixing layer. Proc. Inst. Mech. Eng. G J. Aerosp. Eng. **229**(7), 1349–1359 (2015)
37. L.Y. Jiang, I. Campbell, Prandtl/Schmidt number effect on temperature distribution in a generic combustor. Int. J. Therm. Sci. **48**, 322–330 (2009)
38. G. He, Y. Guo, A.T. Hsu, The effect of Schmidt number on turbulent scalar mixing in a jet in-crossing flow. Int. J. Heat Mass Transf. **42**, 3727–3738 (1999)
39. H. Kaaling, R. Ryden, Y. Bouchie, et al., RQL combustor development including design, CFD calculations, CARS measurements and combustion tests. ISABE pp. 97–7069 (1997)
40. L. Schiller, Z. Naumann, A drag coefficient correlation. VDI Ztg. **77**, 318–320 (1935)
41. K.K. Kuo, *Principles of Combustion* (Wiley, Hoboken, 1986), p. 523
42. A.H. Lefebvre, *Atomization and Sprays* (Hemisphere Publishing Corporation, New York, 1989), pp. 201–221
43. G.N. Abramovich, *Theory of Turbulent Jets* (MIT Press, Cambridge, 1963)
44. A.H. Lefebvre, *Gas Turbine Combustion* (Hemisphere publishing Corporation, New York, 1983)
45. ANSYS, ICEM-CFD-11, Installation and Overview (2007)